

# Triterpenoids from *Protorhus longifolia* Exhibit Hypocholesterolemic Potential via Regulation of Cholesterol Biosynthesis and Stimulation of Low-Density Lipoprotein Uptake in HepG2 Cells

Musawenkosi Ndlovu,\* June C. Serem, Mamoalosi A. Selepe, Andrew R. Opoku, Megan J. Bester, Zeno Apostolides, and Rebamang A. Mosa\*



Cite This: *ACS Omega* 2023, 8, 30906–30916



Read Online

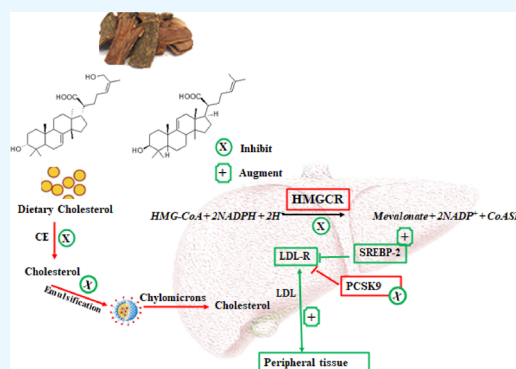
ACCESS |

Metrics & More

Article Recommendations

Supporting Information

**ABSTRACT:** The increasing incidence of hypercholesterolemia-related diseases even in the presence of the currently available cholesterol-lowering drugs indicates a need to discover new therapeutic drugs. This study aimed to investigate the hypocholesterolemic potential of two triterpenoids isolated from *Protorhus longifolia* stem bark. *In silico* techniques and *in vitro* enzyme assays were used to evaluate the potential inhibition of cholesterol esterase and HMG-CoA reductase by the triterpenoids (ARM-2 and RA-5). The toxicity, modulation of low-density lipoprotein (LDL) uptake, and associated gene expression were determined in HepG2 hepatocytes. *In silico* molecular docking revealed that ARM-2 compared with RA-5 has a relatively stronger binding affinity for both enzymes. Both triterpenoids further demonstrated promising *in silico* drug-likeness properties and favorable ADMET profiles characterized by high intestinal absorption and lack of CYP450 enzyme inhibition. The compounds further showed, to varying degrees of efficacy, inhibition of cholesterol micellization as well as both cholesterol esterase and HMG-CoA reductase activities with  $IC_{50}$  values ranging from 16.4 to 41.1  $\mu$ M. Moreover, enhanced hepatic cellular LDL uptake and the associated upregulation of the LDL-R and SREBP-2 gene expression were observed in the triterpenoid-treated HepG2 cells. It is evident that the triterpenoids, especially ARM-2, possess hypocholesterolemic properties, and these molecules can serve as leads or structural templates for the development of new hypocholesterolemic drugs.



## INTRODUCTION

Atherosclerotic cardiovascular diseases (ACVDs) are among the leading contributors to the high rate of mortality worldwide.<sup>1</sup> Persistent elevated levels of blood cholesterol, commonly referred to as hypercholesterolemia, is an independent risk factor for atherosclerosis and related vascular complications. Hypercholesterolemia is characterized by abnormally high plasma total cholesterol and low-density lipoprotein (LDL) levels accompanied by low levels of high-density lipoproteins (HDL). While LDL transports most of the plasma cholesterol to the liver (the major site of LDL receptor (LDL-R) expression) and extra hepatic tissues expressing LDL-R, HDL transports cholesterol from extra hepatic tissues back to the liver for metabolism and clearance. Therefore, high plasma LDL levels are associated with an increased risk of developing ACVDs.<sup>2</sup> Genetic defects in LDL-R and lifestyle factors, including unhealthy eating habits characterized by diets high in saturated fats and cholesterol content, and the lack of regular physical exercise are among the major identified risk factors that instigate hypercholesterolemia.<sup>3</sup>

Different approaches, which include the regulation of dietary cholesterol absorption, endogenous cholesterol biosynthesis,

and plasma LDL levels, have been considered the key in the prevention and management of hypercholesterolemia and its related complications.<sup>4–6</sup> Inhibition of cholesterol esterase and cholesterol micellization are the primary targets for the regulation of dietary cholesterol digestion and absorption. However, since *de novo* cholesterol synthesis is the major source of blood cholesterol, regulation of cholesterol biosynthesis has been considered a crucial step in hypercholesterolemia management. 3-Hydroxy-3-methyl glutaryl coenzyme A reductase (HMGCR), an enzyme that catalyzes the rate-limiting step of cholesterol biosynthesis in the mevalonate pathway, has been the most common target to regulate cholesterol biosynthesis. Statins, which are the commonly used hypolipidemic drugs, competitively inhibit HMGCR to control

Received: March 24, 2023

Accepted: June 16, 2023

Published: August 14, 2023



endogenous cholesterol biosynthesis. Furthermore, the liver removes cholesterol-rich LDL from the blood via receptor-mediated endocytosis through cell surface LDL-R.<sup>7</sup> LDL-R expression is tightly regulated in response to the levels of intracellular cholesterol. Thus, the modulation of hepatic LDL-R expression and stimulation of cellular LDL uptake is desirable for the management of hypercholesterolemia and its related atherosclerotic events.

Currently available plasma cholesterol-lowering drugs, which include statins, ezetimibe, and bile acid sequestrants, have clinical limitations due to the development of various adverse effects such as muscle pains and liver inflammation.<sup>8,9</sup> Statins as the most used lipid-lowering agents have also been reported to have minimal efficacy against the risk of ACVDs likely to develop in patients aged 70 years or older.<sup>10</sup> Due to the limitations associated with the currently available hypocholesterolemic drugs, there is a continuous search for alternative remedies to combat hypercholesterolemia and its associated diseases. Multitarget drugs that can regulate cholesterol absorption, biosynthesis, and plasma clearance could prove to be ideal for hypercholesterolemia management.

Plant-derived triterpenes, due to their diverse bioactivities, have gained interest in the search for new pharmacologically active drugs against human metabolic disorders including hyperlipidemia.<sup>11,12</sup> Some triterpenes including  $3\beta$ -hydroxylanosta-9,24-dien-21-oic acid (RA-5) from *Protorhus longifolia* (Benrh.) Engl. stem bark have previously been reported to possess some bioactivities relevant to antihypercholesterolemia. These include *in vitro* inhibition of some lipid digestive enzymes, bile acid binding capacity, and *in vivo* antihyperlipidemic effect.<sup>13,14</sup> The present study aimed to further investigate the antihypercholesterolemic potential of RA-5 and a newly identified triterpenoid from *P. longifolia* stem bark, using both *in silico* and *in vitro* techniques.

## RESULTS

**Isolation and Characterization of the New Compound.**  $3\beta$ -Hydroxylanosta-9,24-dien-21-oic acid (RA-5) has previously been isolated and characterized from *P. longifolia* stem bark.<sup>15</sup> The newly identified compound ( $3\alpha,26$ -dihydroxytirucalla-7,24-dien-21-oic acid, ARM-2) (Figure 1)

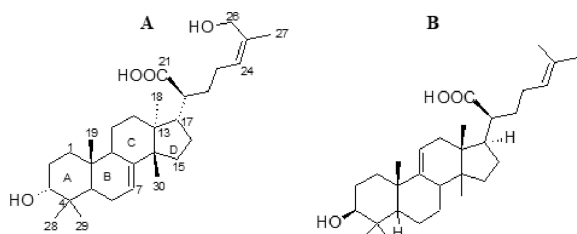


**Figure 1.** Chemical structures of the newly isolated compound ( $3\alpha,26$ -dihydroxytirucalla-7,24-dien-21-oic acid, ARM-2) (A) and ( $3\beta$ -hydroxylanosta-9,24-dien-21-oic acid, RA-5) (B).

was isolated as a white amorphous solid. Its molecular formula was determined to be  $C_{30}H_{48}O_4$  based on its HRESIMS data, which showed a deprotonated molecular ion peak at  $m/z$  471.3480  $[M-H]^-$  (calculated for  $C_{30}H_{47}O_4$ , 471.3474). The NMR data of ARM-2 is presented in Table 1.

The signals that were observed from the  $^1H$  NMR spectrum included six methyl group signals appearing as three-proton singlets at  $\delta_H$  0.825, 0.81, 0.91, 0.822, 0.69, and 1.66 for the

**Table 1.**  $^{13}C$  NMR (125 MHz) and  $^1H$  NMR (400 MHz) Spectral Data for ARM-2 in  $DMSO-d_6$

position	$\delta_C$ , type	$\delta_H$ , mult. ( $J$ in Hz)	HMBC (H $\rightarrow$ C)
1	30.9, CH <sub>2</sub>	1.18–1.28, m; 1.34–1.51, m	C-3, 5, 10
2	25.4, CH <sub>2</sub>	1.75–1.80, m; 1.34–1.51, m	C-3, 4
3	73.9, CH	3.22, brs	C-1, 5
4	37.0, C		
5	43.9, CH	1.69–1.72, m	C-19, 29, 6, 4
6	23.5, CH <sub>2</sub>	1.84–1.98, m	C-8
7	117.9, CH	5.20–5.22, m	C-5, 9, 14
8	145.5, C		
9	48.0, CH	2.20–2.26, m	C-8, 11
10	34.3, C		
11	16.8, CH <sub>2</sub>	1.34–1.51, m	C-9, 13
12	30.0, CH <sub>2</sub>	1.63–1.69, m; 1.34–1.51, m	C-14, 18, 9
13	42.9, C		
14	50.6, C		
15	33.2, CH <sub>2</sub>	1.34–1.51, m	C-17
16	26.6, CH <sub>2</sub>	1.18–1.28, m; 1.84–1.98, m	C-13, 20
17	49.2, CH	1.84–1.98, m	
18	21.4 <sup>a</sup> , CH <sub>3</sub>	0.822 <sup>a</sup> , s	C-12, 13, 14
19	12.9, CH <sub>3</sub>	0.69, s	C-5, 9, 10, 1
20	47.2, CH	2.09, dd (9.1 & 16.2)	C-21, 17
21	176.9, C		
22	32.4, CH <sub>2</sub>	1.34–1.51, m	C-21, 24
23	25.1, CH <sub>2</sub>	1.84–1.98, m; 1.34–1.51, m	C-20, 25
24	125.1, CH	5.12, t (7.2)	C-26, 27
25	135.9, C		
26	59.3, CH <sub>2</sub>	3.86, d (5.3)	C-24, 25, 27
27	21.3 <sup>a</sup> , CH <sub>3</sub>	1.66, s	C-24, 25, 27
28	21.7 <sup>a</sup> , CH <sub>3</sub>	0.825 <sup>a</sup> , s	C-3, 4, 5
29	28.2, CH <sub>3</sub>	0.81 <sup>a</sup> , s	C-3, 4, 5
30	27.0, CH <sub>3</sub>	0.91, s	C-8, 13, 14, 15
OH-21		12.06, s	
OH-26		4.51, t (5.3)	C-26, C-25
OH-3		4.23, d (4.4)	C-3, C-4, C-2

<sup>a</sup>Assignments in the same column may be interchanged.

olefinic methyl, one oxymethine signal at  $\delta_H$  3.22 (brs), one oxymethylene signal at  $\delta_H$  3.86 (d,  $J = 5.3$  Hz), two vinylic methine signals at  $\delta_H$  5.20–5.22 (m) and 5.12 (t,  $J = 7.2$  Hz), and four methine signals at  $\delta_H$  2.09 (dd,  $J = 9.1$  and 16.2 Hz), 2.20–2.26 (m), 1.84–1.98 (m), and 1.69–1.72 (m). The methylene signals resonated at  $\delta_H$  1.75–1.80 (m), 1.84–1.98 (m), 1.34–1.51 (m), and 1.18–1.28 (m). In addition, signals of three hydroxy groups appeared at  $\delta_H$  12.06 (s), 4.51 (t,  $J = 5.3$  Hz), and 4.23 (d,  $J = 4.4$  Hz). The appearance of the hydroxy signal at  $\delta_H$  12.06 (s) indicated the presence of a carboxyl group in the molecule. The  $^{13}C$  and dept-135 NMR spectra showed six methyl signals at  $\delta_C$  12.9, 21.4, 21.3, 21.7, 28.2, and 27.0, seven methine signals that included an oximethine ( $\delta_C$  73.9), olefin carbons at  $\delta_C$  117.9 and 125.1, and the methine carbons at  $\delta_C$  43.9, 47.2, 48.0, and 49.2. In the  $^{13}C$  NMR spectrum, 10 methylene signals were also present, which resonated at  $\delta_C$  30.9, 25.4, 23.5, 16.8, 30.0, 33.2, 26.6, 32.4, 25.1, and 59.3 (for the oxymethylene). Seven signals of non-hydrogenated carbons that included four quaternary carbon signals ( $\delta_C$  37.0, 34.3, 42.9, and 50.6), two tertiary carbon signals ( $\delta_C$  145.5 and 135.9), and the signal of the carboxyl group ( $\delta_C$  176.9) were observed.

The assignment of the signals was facilitated by 2D NMR spectroscopy that included COSY, HSQC, and HMBC. The

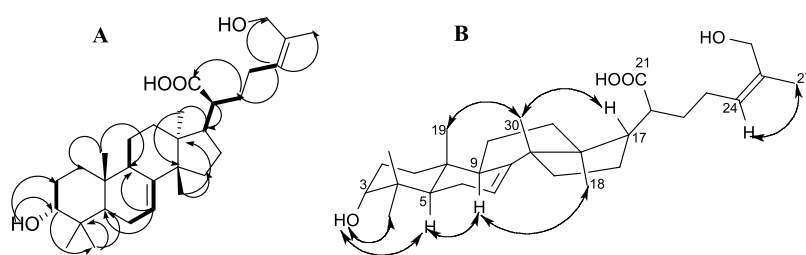


Figure 2. Key COSY (bold face) and HMBC (arrows) correlations (A) and Key ROESY correlations (B) of ARM-2.

Table 2. XP Glide Scores of ARM-2, RA-5, Lovastatin, and Simvastatin for Cholesterol Esterase (2BCE) and HMG-CoA Reductase (1DQ8)

ligand	cholesterol esterase			HMG-CoA reductase		
	catalytic site	allosteric site 1	allosteric site 2	catalytic site	allosteric site 1	allosteric site 2
ARM-2	−8.108	−7.207	−3.806	−7.535	−4.885	−5.453
RA-5	−6.924	−5.871	−2.555	−4.279	−4.337	−4.227
simvastatin	−7.854	−6.340	−3.933	−5.402	−4.495	−3.841
lovastatin	−7.845	−6.795	−2.776	−6.518	−4.786	−4.841
<i>p</i> -NPB	−3.777	−3.031	−1.645			
HMG-CoA				−11.387	−10.889	−9.820

Table 3. Physicochemical and Medicinal Chemistry Properties of the Triterpenoids Predicted by the Swiss-ADME Webserver<sup>a</sup>

compound	MW (g/mol)	TPSA (Å <sup>2</sup> )	MR	Lipinski	lipophilicity (Log Po/w)	bioavailability score	PAINS alert	lead-likeness
RA-5	457.70	57.53	138.81	yes*	6.27	0.85	0	no**
ARM-2	471.34	77.76	140.24	yes*	4.87	0.56	0	no**
simvastatin	418.57	72.83	118.47	yes	4.13	0.55	0	no**
lovastatin	404.54	72.83	113.92	yes	3.81	0.55	0	no**

<sup>a</sup>MW: molecular weight; MR: molar refractivity; TPSA: topological surface area; \*1 violation MLOGP>4.15, \*\* 2violations MW > 350, XLOGP3 > 3.5, \*\*\* 3 violations MW > 350, XLOGP3 > 3.5, Rotors >7.

COSY correlation from H-3 ( $\delta_{\text{H}}$  3.22) to H<sub>2</sub>-2 [ $\delta_{\text{C}}$  1.75–1.80 (m) and 1.34–1.51 (m)] together with HMBC correlations from H-3 to C-1 ( $\delta_{\text{C}}$  30.9, CH<sub>2</sub>) and C-5 ( $\delta_{\text{C}}$  43.9, CH), from H<sub>3</sub>-28 and H<sub>3</sub>-29 to C-3 ( $\delta_{\text{C}}$  73.9, CH), C-4 (37.0, C), and C-5 ( $\delta_{\text{C}}$  43.9, CH), and from H-5 ( $\delta_{\text{H}}$  1.69–1.72) to C-4 ( $\delta_{\text{C}}$  37.0, C) and C-19 ( $\delta_{\text{C}}$  12.9, CH<sub>3</sub>) led to the establishment of the A-ring of the triterpenoid (Figure 2A). The COSY correlations from H-7 ( $\delta_{\text{H}}$  5.20–5.22) to H<sub>2</sub>-6 ( $\delta_{\text{H}}$  1.84–1.98) and H-9 ( $\delta_{\text{H}}$  2.20–2.26), together with the HMBC correlations from H-7 ( $\delta_{\text{H}}$  5.20–5.22) to C-5 ( $\delta_{\text{C}}$  43.9, CH), C-9 ( $\delta_{\text{C}}$  48.0, CH), and C-14 ( $\delta_{\text{C}}$  50.6, C) confirmed the endocyclic double bond situated at C-7 and C-8 of the B-ring. The HMBC correlations from H<sub>3</sub>-30 ( $\delta_{\text{H}}$  0.91) to C-8 ( $\delta_{\text{C}}$  145.5, C), C-13 ( $\delta_{\text{C}}$  42.9, C), and C-15 ( $\delta_{\text{C}}$  33.2, CH<sub>2</sub>) and those from H<sub>3</sub>-18 ( $\delta_{\text{H}}$  0.822) to C-12 ( $\delta_{\text{C}}$  30.0, CH<sub>2</sub>), C-14 ( $\delta_{\text{C}}$  50.6, C), and C-17 ( $\delta_{\text{C}}$  49.2, CH) were indicative of the additional two ring systems, the C- and D-rings. The linkage of the eight-carbon side chain to C-17 was assigned based on the COSY correlations from H-20 ( $\delta_{\text{H}}$  2.09, dd,  $J$  = 9.1 & 16.2 Hz) to H<sub>2</sub>-22 ( $\delta_{\text{H}}$  1.34–1.51) and H-17 ( $\delta_{\text{H}}$  1.84–1.98). This was further corroborated by the HMBC correlations from H-20 to C-17 ( $\delta_{\text{C}}$  49.2, CH) and C-21 ( $\delta_{\text{C}}$  176.9, C) as well as HMBC correlations from the olefinic methine at  $\delta_{\text{H}}$  5.12 (t,  $J$  = 7.2 Hz, H-24) to C-22 ( $\delta_{\text{C}}$  32.4, CH<sub>2</sub>), C-26 ( $\delta_{\text{C}}$  59.3, CH<sub>2</sub>), and C-27 ( $\delta_{\text{C}}$  21.3, CH<sub>3</sub>) (Figure 2A). These indicated that the side chain consisted of 2-methylbutenol linked to propionic acid fragments. The relative configuration was determined from ROESY spectrum and analysis of the splitting patterns of the proton signals. The appearance of H-3 as a broad singlet suggested an  $\alpha$ -orientation of OH-3. This was corroborated by

ROESY correlations from OH-3 to H-5 (Figure 2B). The ROESY correlations from H-9 to H-5 and H<sub>3</sub>-18 and from H<sub>3</sub>-18 to H-20 indicated that H-5, H-9, H-20, and H<sub>3</sub>-18 were all on the same face and  $\alpha$ -oriented. The ROESY correlation from H<sub>3</sub>-30 to H-17 and from H<sub>3</sub>-19 to H<sub>3</sub>-30 indicated that H<sub>3</sub>-19, H<sub>3</sub>-30, and H-17 were  $\beta$ -oriented. The *Z* configuration of the double bond at C-24 and C-25 was established from the ROESY correlations of H-24 to H<sub>3</sub>-27. These assignments indicate that the compound is structurally similar to the known compound 3- $\alpha$ -hydroxy-7,24-diene-tirucallic acid<sup>16</sup> except that one of the alkenyl methyl groups is a methyl alcohol in compound ARM-2. Therefore, ARM-2 is named 3 $\alpha$ ,26-dihydroxytirucalla-7,24-dien-21-oic acid. The spectra of the compound are presented in the Supporting Information.

**Molecular Docking Studies.** Molecular docking analysis was performed to predict and understand the binding modes of the triterpenoids on cholesterol esterase and HMG-CoA reductase. Glide scores of the triterpenes and the selected reference drugs, ranked according to Glide XP score, are presented in Table 2. Both triterpenoids were predicted to have stronger binding affinities at the catalytic site and allosteric site 1 of cholesterol esterase than HMG-CoA reductase. The docking scores of ARM-2 are highly comparable to those of simvastatin and lovastatin.

**Drug-Likeness and ADMET Predictions of ARM-2 and RA-5.** SWISS-ADME and pkCSM online web servers were used in this study to predict the pharmacokinetic behavior of the triterpenes (ARM-2 and RA-5). Both servers predict the drug-likeness properties of compounds with the help of Lipinski's rule of five. Table 3 presents the physicochemical

**Table 4. ADMET Parameters of the Triterpenes and Simvastatin Predicted by pkCSM<sup>a</sup>**

property	model name	RA-5	ARM-2	simvastatin	reference
absorption	water-soluble (log mol/L)	-4.452	-4.564	-5.162	
	Caco2 permeability (log Papp in 10 <sup>-6</sup> cm/s)	1.480	0.623	0.865	>0.90] high permeability
	intestinal absorption human (% absorbed)	93.643	93.074	94.339	< [30% poor absorbed]
distribution	BBB permeability (log BB)	-0.397	-0.694	-0.26	LogBB > 0.3 highly D, LogBB < -1 poorly D
	CNS (log PS)	-1.271	-1.776	-2.095	LogPS > -2 penetrate, LogPS < -3 unable
metabolism	CYP3A4 substrate	yes	yes	yes	categorical (yes/no)
	CYP2C9 inhibitor	no	no	no	categorical (yes/no)
	CYP3A4 inhibitor	no	no	yes	categorical (yes/no)
excretion	total clearance (log ml/min/kg)	0.317	0.451	0.827	
	renal OCT2 substrate	no	no	yes	categorical (yes/no)
toxicity	AMES toxicity	no	no	no	categorical (yes/no)
	hepatotoxicity	yes	yes	no	categorical (yes/no)

<sup>a</sup>ADMET, absorption, distribution, metabolism, excretion, and toxicity; Papp, apparent permeability coefficient; AMES, assay of the ability of a chemical compound to induce mutations in DNA; BBB, blood–brain barrier; BB, blood–brain; CNS, central nervous system; PS, permeability–surface area.

**Table 5.  $K_m$ ,  $V_{max}$ ,  $K_i$ , and the Mode Inhibition of RA-5 and ARM-2 on the Inhibition of Cholesterol Esterase and HMG-CoA Reductase<sup>a</sup>**

inhibitor	IC <sub>50</sub> (μM)	$K_m$ (μM)	$V_{max}$ (μM)	$K_i$ (μM)	mode of inhibition
Cholesterol esterase					
RA-5	16.36 ± 1.31 <sup>#</sup>	0.086 ± 0.017	0.140 ± 0.042	4.98 ± 0.40	mixed
ARM-2	18.38 ± 4.09 <sup>#</sup>	0.019 ± 0.004	0.079 ± 0.022	6.45 ± 0.70	mixed
simvastatin	25.68 ± 2.89	0.004 ± 0.003	0.014 ± 0.011	4.03 ± 0.18	competitive
control		0.01 ± 0.05	0.089 ± 0.032		
HMG-CoA reductase					
RA-5	41.09 ± 1.07*	0.041 ± 0.31	0.034 ± 0.013	170 ± 4.67	mixed
ARM-2	26.62 ± 7.16	0.135 ± 0.04	0.037 ± 0.021	39.7 ± 1.19	mixed
lovastatin	34.32 ± 7.93	0.185 ± 0.067	0.052 ± 0.003	49.08 ± 1.15	competitive
control		0.056 ± 0.002	0.052 ± 0.001		

<sup>a</sup>Data are expressed as the mean ± SEM,  $n = 3$  \* $p < 0.05$  versus lovastatin, <sup>#</sup> $p < 0.05$  simvastatin.

and medicinal chemistry properties of the triterpenoids predicted by the Swiss-ADME webserver. The results revealed that both compounds obey Lipinski's rule. While the bioavailability score of ARM-2 was predicted to be equal to those of the reference drugs (simvastatin and lovastatin), RA-5 showed a slightly higher bioavailability score. Similar to the selected reference drugs, both triterpenoids were also predicted to have zero PAINS alerts.

The ADMET profiles of ARM-2 and RA-5 are presented in Table 4. The triterpenoids were predicted to be easily absorbed from the intestines with a magnitude comparable to that of simvastatin. This was further supported by the predicted high Caco2 permeability (RA-5: 1.48, ARM-2: 0.623, and simvastatin: 0.866 log Papp in 10<sup>-6</sup> cm/s). Both triterpenoids can cross both the BBB and CNS. While both compounds were predicted to be substrates of CYP3A4, both were found not to inhibit CYP2C9 and CYP3A4. The triterpenes were further predicted not to be Renal OCT2 substrates, mutagenic with no AMES predicted. However, RA-5 was predicted to be potentially hepatotoxic.

**In Vitro Enzyme Inhibition.** *In vitro* bioassays were performed to confirm the *in silico* molecular docking results related to the potential inhibition of ARM-2 and RA-5 on cholesterol esterase and HMG-CoA reductase activity. Findings (Table 5) showed that both triterpenoids exhibit inhibitory effects against the two enzymes. Interestingly, for both enzymes, both triterpenoids showed a relatively higher potency than simvastatin. For HMG-CoA reductase inhibition,

the IC<sub>50</sub> value of ARM-2 (26.62 μM) was lower than that of lovastatin (34.32 μM).

The double-reciprocal Lineweaver–Burk plots (Figure 3) revealed that the triterpenoids inhibit cholesterol esterase in a mixed type of inhibition as the  $V_{max}$  was the same as the control (no inhibitor), with different  $K_m$  values (Table 5). The calculated dissociation constant ( $K_i$ ) for RA-5 (4.98 μM) was comparable to that for simvastatin (4.03 μM), while the  $K_i$  for ARM-2 (6.45 μM) was significantly different when compared with RA-5 and simvastatin. It is evident that the triterpenoids possess a mixed type of inhibition against HMG-CoA reductase when compared with lovastatin, which competitively inhibits the enzyme. While the binding affinity of RA-5 (170 μM) to the free enzyme was higher than that of lovastatin (49.08 μM), interestingly, ARM-2 (39.7 μM) showed a lower binding affinity when compared with the reference standard lovastatin (Table 5).

**Cholesterol Micellization Inhibition.** The effects of ARM-2 and RA-5 with gallic acid as the control on cholesterol micellization were also determined, and the results are presented in Figure 4. A relatively higher cholesterol concentration in the sample control was significantly ( $p \leq 0.0001$ ) reduced in the triterpenoid treated samples (Figure 4A). A concentration-dependent inhibition of cholesterol micellization (Figure 4B) was observed. The inhibitory effect of the triterpenoids, especially ARM-2, was comparable to that of gallic acid, the reference control. The IC<sub>50</sub> values of gallic

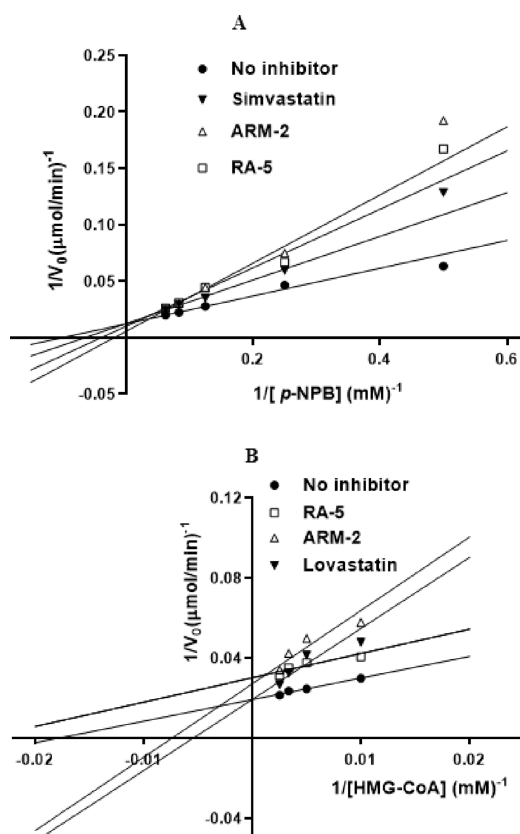


**Figure 3.** Lineweaver–Burk plots for cholesterol esterase (A) and HMG-CoA reductase (B) and inhibition.  $1/V_{\max}$ : reciprocal of maximum velocity;  $1/[S]$ : reciprocal of substrate concentration.

acid, ARM-2, and RA-5 were  $9.40 \pm 3.815 \mu\text{M}$ ,  $16.57 \pm 2.01 \mu\text{M}$ , and  $25.12 \pm 2.19 \mu\text{M}$ , respectively.

**ARM-2 and RA-5 Enhance Cellular LDL Uptake in HepG2 Cells.** An LDL-DyLight uptake assay in HepG2 cells was used to investigate the effect of the triterpenoids on hepatic LDL uptake. A relatively higher cellular LDL uptake, that was concentration-dependent, was observed in HepG2 cells treated with ARM-2 and RA-5 when compared with the control cells. At the highest concentration of  $100 \mu\text{M}$ , ARM-2 and RA-5 significantly stimulated the cellular LDL uptake by 31 and 39%, respectively (Figure 5A). Interestingly, the triterpenoids showed no significant difference in comparison to both lovastatin and simvastatin. Moreover, the triterpenoids

showed no cytotoxic effects up to  $100 \mu\text{M}$  on HepG2 cells (Figure 5B).

**ARM-2 and RA-5 Upregulate LDL-R and SREBP-2 mRNA Levels while Downregulating HMGCR and PCSK9 mRNA Levels in HepG2 Cells.** The effect of the compounds on the expression of some genes (*LDL-R*, *SREBP-2*, *PCSK9*, and *HMGCR*) associated with cellular LDL uptake was also investigated in HepG2 cells. As shown in Figure 6A,B, relatively higher mRNA levels of the *LDL-R* and *SREBP-2* genes were observed in the cells treated with the triterpenoids ( $100 \mu\text{M}$ ) in comparison to the control. While the *LDL-R* mRNA was upregulated by up to 0.5- and 0.48-fold relative to the control cells, RA-5 (at  $100 \mu\text{M}$ ) also showed up to 0.4-fold change ( $p < 0.05$ ) on *SREBP-2* mRNA. The cell treatment with the triterpenoids (at  $100 \mu\text{M}$ ) further significantly ( $p \leq 0.001$ ,  $p \leq 0.0001$ ) reduced the expression of the *HMGCR* gene by 0.4-fold (39.8%) and 0.5-fold (45.3%) for ARM-2 and RA-5, respectively, when compared with the control (Figure 6D). Furthermore, the cells treated with the lower concentration ( $25 \mu\text{M}$ ) of both triterpenoids showed increased expression of *PCSK9* gene when compared with the control. However, an insignificant decrease in gene expression was observed for the cells treated with RA-5 and ARM-2 at  $100 \mu\text{M}$  when compared to the control (Figure 6C). Interestingly, there was no significant difference between the statins and the triterpenoids at  $100 \mu\text{M}$ .

**Protein–Protein Interactions.** The PPI network of the genes that were upregulated (*LDL-R* and *SREBP-2*) or downregulated (*HMGCR* and *PCSK9*) by the tested triterpenoids was constructed using the STRING database (Figure 7A). The network is shown in nodes where each node represents a protein and its structure. The nodes are connected by edges and each edge represents protein–protein associations, including known, predicted, and other interactions. A total of six edges were constructed between the nodes revealing different types of interactions between the four genes (Figure 7A). The average node degree of freedom is 3, and the average local clustering coefficient is 1. Further analysis of the PPI network obtained from STRING was performed by Cytoscape software, and the degree of core expression is represented as the thickness of the edges (Figure 7B). The results reveal that the genes are interconnected, suggesting that regulation of one gene may lead to regulation of another gene.

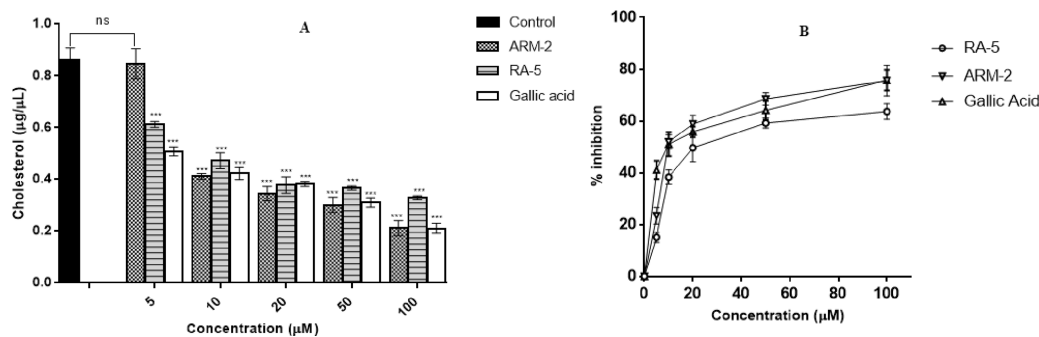


**Figure 4.** Effect of the triterpenoids on cholesterol micellization. Cholesterol levels in the generated micelle (A) and inhibitory effect (%) of the triterpenoids on cholesterol micellization (B). Gallic acid was used as a reference compound. Data are expressed as the mean  $\pm$  SD,  $n = 3$  \*\*\* $p \leq 0.0001$  versus control.

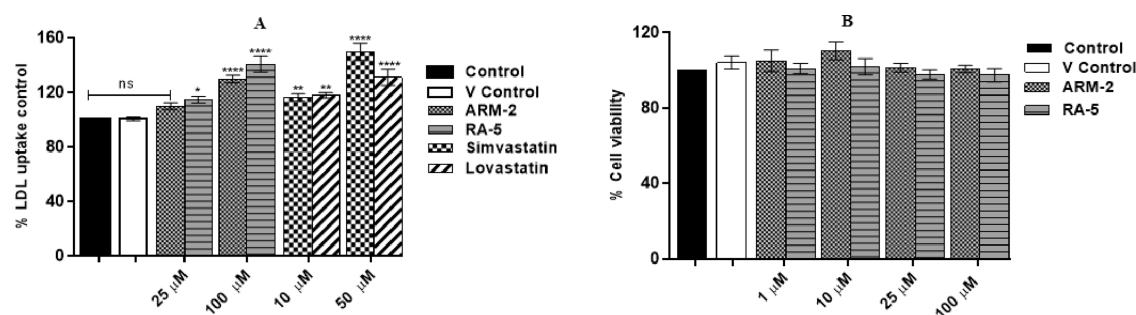


**Figure 5.** Effect of the triterpenoids on LDL-uptake in HepG2 cells (A). The cells were exposed to LDL-DyLight (for 2 h at 37 °C) in the presence and absence of the triterpenoids at 25 and 100  $\mu\text{M}$ . Lovastatin and simvastatin (at 10 and 50  $\mu\text{M}$ ) were used as positive controls. The percentage cell number was unchanged after 72 h exposure to the triterpenoids (B). While the model control cells were exposed to PBS only, the vehicle control cells were exposed to methanol ( $\leq 0.01\%$ ). Values are expressed as mean  $\pm$  SEM,  $n = 3$  independent biological repeats in triplicates, \* $p < 0.05$ , \*\* $p < 0.01$ , \*\*\* $p \leq 0.001$  versus control.

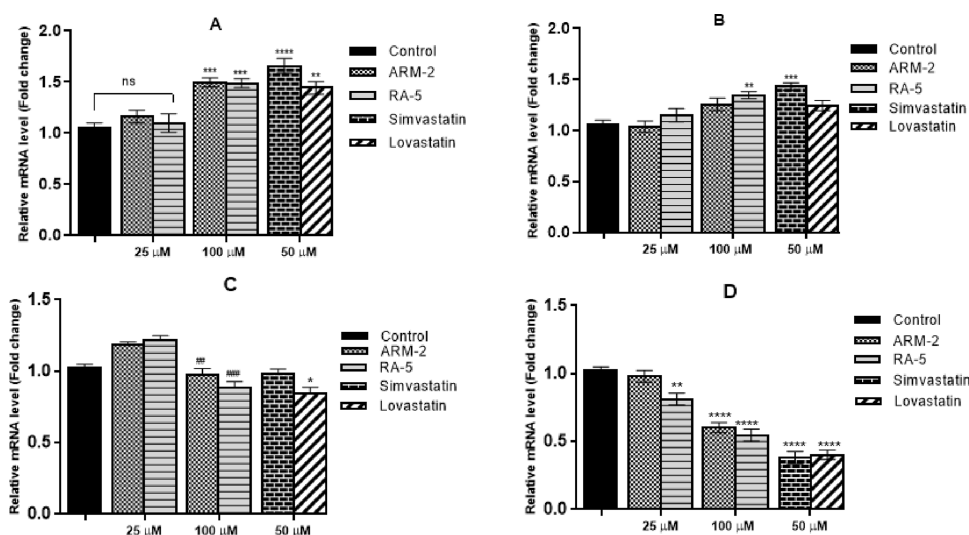


**Figure 6.** Effect of ARM-2 and RA-5 on *LDL-R* (A), *SREBP-2* (B), *PCSK9* (C), and *HMGCR* (D) mRNA levels in HepG2 cells. The cells were exposed to LDL-DyLight (for 2 h at 37 °C) in the presence and absence of the triterpenoids at 25 and 100  $\mu\text{M}$ . Lovastatin and simvastatin (at 50  $\mu\text{M}$ ) were used as positive controls. Data were expressed as the mean  $\pm$  SEM,  $n = 3$  independent biological experiments (each experiment carried out in triplicates), \* $P < 0.05$ , \*\* $P < 0.01$ , \*\*\* $P \leq 0.001$  vs untreated cells group and ## $P < 0.01$ , ### $P \leq 0.001$  vs 25  $\mu\text{M}$  (ARM-2 and RA-5).

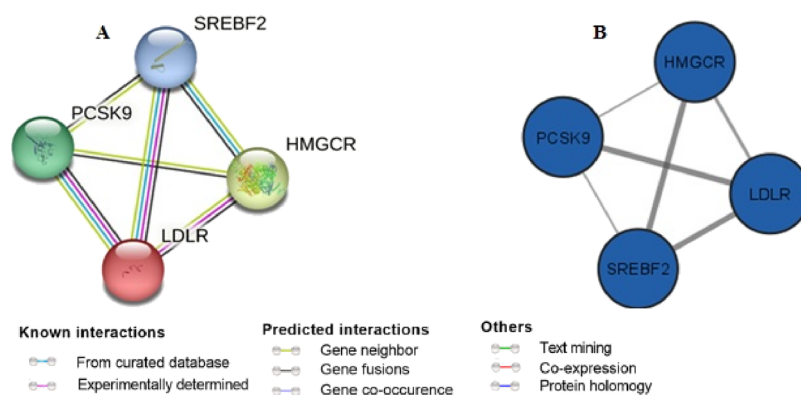


**Figure 7.** Protein–protein interactions (PPIs) of genes that were upregulated and downregulated by the triterpenoids in q-RT-PCR analysis. The PPI network was constructed by importing four overlapping genes and analyzing their interactions using the search tool from the STRING database (A). The association of proteins was constructed by Cytoscape 3.9.1 (B). Proteins are represented by nodes with blue circles, while the edges indicate an association between the proteins.

## DISCUSSION

Elevated blood cholesterol levels are strongly associated with the development and progression of atherosclerotic events leading to serious cardiovascular diseases. Research aiming at

finding alternative solutions to the threat posed by hypercholesterolemia and prevent related health complications is necessary. Plant sterols including triterpenoids have been reported to possess a hypocholesterolemic effect.<sup>17</sup> In the

present study, the hypocholesterolemic potential of two triterpenoids derived from *P. longifolia* was investigated using both *in silico* and *in vitro* techniques. While RA-5 has previously been reported to possess some bioactivities relevant to the hypocholesterolemic effect,<sup>14</sup> ARM-2 is a new tricyclic triterpenoid isolated and reported for the first time from *P. longifolia*.

Molecular docking, a computational tool that provides solid information about protein–ligand interaction and binding modes, has created a new rational approach that significantly reduces time and cost for drug discovery and design. The *in silico* molecular docking of the triterpenoids was performed on cholesterol esterase and HMGCR. The observed high binding affinity of both triterpenoids for the catalytic sites of cholesterol esterase and HMGCR (Table 2) predicted great potential for the compounds to inhibit both enzymes. Based on the predicted binding affinities on both catalytic site and allosteric sites, the compounds could possibly inhibit cholesterol esterase and HMGCR in a mixed type of inhibition manner. While inhibition of cholesterol esterase would limit the digestion and absorption of dietary cholesterol, inhibition of HMGCR would inhibit endogenous cholesterol biosynthesis. Statins exert their hypocholesterolemic effect by competitively inhibiting HMGCR, thus reducing cholesterol biosynthesis.

*In vitro* enzyme bioassays were then undertaken to confirm and further explore the *in silico* findings. The relatively lower IC<sub>50</sub> and K<sub>i</sub> values for RA-5 and ARM-2 for both enzymes (Table 4) indicate the potential potency of enzyme inhibition by the plant compounds. Interestingly, the observed inhibitory effect of RA-5 on cholesterol esterase is consistent with a report,<sup>14</sup> with the current study further revealing the mode of enzyme inhibition by the compound. The observed mixed type of inhibition *in vitro* indicates that either RA-5 or ARM-2 can compete with the substrate for the catalytic site or bind to the allosteric site of the enzymes.

In addition to cholesterol esterase inhibition, the ability of the triterpenoids to inhibit cholesterol micellization further indicated the hypocholesterolemic potential of the compounds. While the observed cholesterol micellization inhibition could partly be linked to their cholesterol esterase inhibitory activity, this could also be associated with the bile acid binding capacity of RA-5 *in vitro* as has been previously identified.<sup>14</sup> In the small intestines, the mixed micellization of dietary triglycerides and cholesterol with secreted bile acids is necessary for efficient digestion and absorption of the lipids. Pharmacologic agents that have bile acid binding properties disrupt micelle formation, thus inhibiting cholesterol absorption.<sup>18</sup>

Furthermore, any molecules that are able to modulate hepatic LDL-R expression and stimulate cellular LDL uptake are desirable for the management of hypercholesterolemia. Interestingly, the observed stimulation of LDL uptake in HepG2 cells by the tested triterpenes (Figure 5) indicates a function related to the potential stimulation of hepatic plasma cholesterol clearance. The activity of the compounds could partly be linked to their ability to upregulate the expression of the *LDL-R* and *SREBP-2* genes (Figure 6A,B). *SREBP-2* is known to control cholesterol homeostasis via transcriptional regulation of *LDL-R gene* and HMG-CoA reductase.<sup>19</sup> Moreover, while the transcriptional expression of *LDL-R* is regulated by *SREBP-2*, in post-translational pathways, *LDL-R* is regulated by protein convertase subtilisin/kexin type 9 (*PCSK 9*). *PCSK 9* mediates *LDL-R* degradation and

interferes with its receptor recycling.<sup>7,20</sup> Although the triterpenoids showed no significant differences in the levels of expressed *PCSK 9* mRNA expression levels, *LDL-R* regulation can still occur via the *LDL-R/SREBP-2* pathway. It is also worth noting that the tested triterpenoids did not only show the potential to inhibit HMGCR activity but also downregulated the expression of the *HMGCR* gene in the HepG2 cells, further confirming the potential of AR-5 and ARM-2 as drugs for the control of cholesterol metabolism.

To qualify as drug candidates, newly discovered compounds should obey Lipinski's rule of 5<sup>21</sup> and have zero PAINS alerts. PAINS alerts predict the stability, reactivity, and toxicity present in the structure of the compound. The tested triterpenoids obey the Lipinski's rule of 5 with zero PAINS alerts (Table 3) and qualify as potential drug candidates. Drug-likeness is further supported by the predicted favorable ADMET profile characterized by high intestinal absorption regardless of poor water solubility, lack of CYP450 enzyme inhibition, mutagenicity, and toxicity (Table 4). CYP450 and isoforms are detoxifying enzymes central to drug metabolism, and inhibition of these enzymes can lead to toxicity.<sup>22,23</sup> Despite the *in silico* predicted hepatotoxicity, no RA-5 (at 100  $\mu$ M) cytotoxicity was observed in HepG2 cells.

## CONCLUSIONS

The findings of this study revealed that both triterpenoids, RA-5 and ARM-2, exhibit antihypercholesterolemic potential. In addition to potential inhibition of dietary cholesterol digestion and absorption as well as modulation of hepatic clearance of plasma cholesterol-rich LDL, both plant compounds could potentially regulate endogenous cholesterol biosynthesis. The triterpenoids could serve as lead molecules or structural templates in the development of new hypocholesterolemic drugs. The *in vivo* antihypercholesterolemic effect of the triterpenoids is recommended for future study.

## MATERIALS AND METHODS

**Reagents.** Cholesterol esterase from *Pseudomonas* sp., 3-HMG-CoA reductase human, 3-HMG-CoA human, 4-nitrophenyl butyrate (NPB), cholesterol, L- $\alpha$ -phosphatidylcholine, oleic acid, lovastatin, cholesterol assay kit (MAK043-1KT),  $\beta$ -nicotinamide adenine dinucleotide (NAD<sup>+</sup>), simvastatin, 1,4-dithiothreitol (DTT), taurocholic acid sodium salt hydrate, gallic acid, and EDTA disodium salt dihydrate were purchased from Sigma-Aldrich (St Louis, Missouri, USA) and Glenthams LS (Corsham, United Kingdom). Oligo primers (Inqaba Biotech, RSA), LDL uptake Kit (ab236208 Abcam), SV Total RNA Isolation (Z3100), and Go Taq qPCR Master Mix (A6001) (Promega) (USA, Madison, Wisconsin, USA) were used.

**Plant Material and Extraction.** The fresh stem barks of *P. longifolia* were collected (in June 2019) at Kwa-Hlabisa, KwaZulu Natal. The plant specimen (voucher specimen number RA01UZ) was deposited at the University of Zululand herbarium. The plant material was air-dried and ground to powder. The powdered plant material (5 kg) was sequentially extracted (1:5 w/v) with *n*-hexane and chloroform. The obtained extracts were separately concentrated under reduced pressure at 40 °C using a rotary evaporator (Heidolph, Instruments Heidolph.Laborota 4000) to afford the hexane and chloroform crude extracts.

**Isolation of Compounds.** The bioactive compounds were isolated from the chloroform extract of the plant material using silica gel column chromatography.<sup>14</sup> The chloroform extract (15 g) was subjected to silica gel column chromatography. The column was eluted stepwise with an *n*-hexane-ethyl acetate solvent system (9:1 → 8:2 → 7:3 → 6:4 → 4:6 → 3:7 → 2:8). Thin-layer chromatography (silica gel 60 TLC aluminum sheets, F<sub>254</sub>, Merck, Darmstadt, Germany) was used to analyze the collected fractions (20 mL). The collected fractions with similar profile were combined to give Fractions A to T. Fractions H and Q were concentrated and recrystallized in hexane and ethyl acetate, respectively, to yield RA-5 (0.86 g) and ARM-2 (1.38 g). The chemical structures of RA-5 and ARM-2 were obtained based on spectral data analysis and by comparing the data with literature values.<sup>14,15</sup> The NMR spectra were recorded at ambient temperature on a Bruker Avance III 400 spectrometer equipped with a BBI probe and an Avance III HD 500 spectrometer with a Prodigy probe. <sup>1</sup>H and <sup>13</sup>C NMR chemical shifts were referenced to residual and solvent peaks at  $\delta_{\text{H}}$  7.26,  $\delta_{\text{C}}$  77.0 for CDCl<sub>3</sub> and  $\delta_{\text{H}}$  2.50,  $\delta_{\text{C}}$  39.52 for (CD<sub>3</sub>)<sub>2</sub>SO. Chemical shifts are reported in ppm ( $\delta$ ) and coupling constants (*J*) in Hz. The HRESIMS data were acquired on a UPLC coupled to QTOF Synapt G2 HDMS (Waters Corp., MA, USA) operating in both positive and negative electrospray ionization (ESI) modes.

**Molecular Docking of the Compounds.** The molecular docking of the isolated compounds against cholesterol esterase (2BCE) and HMG-CoA reductase (1DQ8) was evaluated using Maestro from Schrodinger (2022\_1). Three-dimensional crystal structures of the proteins (enzymes) were obtained from the RCSB Protein Data Bank (PDB). The proteins and ligands (test compounds) were all prepared on Maestro. Site mapping on Maestro was accessed to explore the catalytic and allosteric sites of the enzymes. ChemDraw Ultra 6.0 software was used to draw the structures of the triterpenoids and convert them to 3D formats. Docking calculations of the structure–protein interaction were carried out using Maestro from Schrodinger.

**Prediction of Pharmacokinetics and Physicochemical Properties of the Triterpenes.** pkCSM (<http://structure.bioc.cam.ac.uk/pkcsml>) and Swiss-ADME (<http://www.swissadme.ch>) webserver were accessed to investigate the physicochemical and pharmacokinetics (absorption, distribution, metabolism, excretion, and toxicity (ADMET)) properties of the triterpenoids. pkCSM is an accessible webserver that uses graph-based signatures to represent small-molecule chemistry and topology vital to develop predictive models of central ADMET properties for drug development.<sup>24</sup> The physicochemical parameters predicted include molecular weight, topological polar surface area (TPSA), number of H-bond acceptors, and lipophilicity.

**In Vitro Assays. Cholesterol Esterase Inhibition Assay.** The cholesterol esterase inhibitory activity of the compounds was determined using *p*-nitrophenyl butyrate (*p*-NPB) as an artificial substrate.<sup>25</sup> The reaction mixture containing 24 mM taurocholic acid, 8 mM *p*-NPB, test compound (5–100  $\mu$ M), and 0.1 M sodium phosphate buffer, pH 7.0, was preincubated at 37 °C for 10 min. The reaction was initiated by adding 1.25  $\mu$ g/mL cholesterol esterase, and the reaction mixture was incubated at 37 °C for 15 min. Simvastatin was used as a reference drug in place of the test compound. The enzyme activity was determined by calorimetrically measuring the release of *p*-nitrophenol (as a yellow-colored product).

Absorbance was read at a wavelength of 405 nm using a SpectraMax paradigm microplate reader (Molecular Devices Inc., San Jose, California).

**HMG-CoA Reductase Inhibition Assay.** The HMG-CoA reductase inhibition assay described by ref 26 was followed to determine the inhibitory activity of the triterpenoids on HMG-CoA reductase. Briefly, the reaction mixture comprised triterpenoid (5–100  $\mu$ M), 400  $\mu$ M HMG-CoA, 400  $\mu$ M NADPH, and 100 mM potassium phosphate buffer pH 7.4 [containing 120 mM KCl, 5 mM DTT and 1 mM EDTA]. Simvastatin and lovastatin were used as reference drugs in place of the test compound. The reaction was initiated by the addition of HMG-CoA reductase (0.17 mg/mL). The reaction mixture was incubated at 37 °C for 10 min, and absorbance was measured at 340 nm using the SpectraMax paradigm microplate reader.

**Enzyme Kinetics.** To investigate the modes of inhibition, the enzymatic assays were performed according to the abovementioned reaction protocols. While all other parameters remained unchanged, the enzyme activity was measured at increasing respective substrates concentrations (cholesterol esterase: 2–10 mM and HMG-CoA reductase: 100–500  $\mu$ M) in the presence and absence of the test compound (inhibitor). Lineweaver–Burk reciprocal plots were generated and used to determine the inhibition type,  $K_{\text{m}}$ , and  $V_{\text{max}}$ . The inhibitory constants ( $K_{\text{i}}$ ) of the test compounds were also calculated.

**Inhibition of Cholesterol Micellization.** Artificial micelles were prepared following the method described by ref 27 with slight modifications. The micelles were prepared by dissolving 2 mM cholesterol, 1 mM oleic acid, and 2.4 mM phosphatidylcholine in methanol. The lipid mixture was mixed well and then dried by allowing methanol to evaporate. The dried mixture was redissolved in 15 mM sodium phosphate buffer pH 7.4, containing 6.6 mM taurocholate salt and 132 mM NaCl. The emulsion was sonicated for 30 min and incubated overnight at 37 °C for micelle formation. After incubation, the test compound (5–100  $\mu$ M) was added followed by a second sonication and incubation for 1 h at 37 °C. The solution was centrifuged at 1000g for 10 min, and the supernatant was collected for determination of free cholesterol concentration. The cholesterol concentration was determined using a cholesterol test kit (Sigma Aldrich) following the instructions of the kit manufacturer.

**Inhibitory Activity and IC<sub>50</sub> Determination.** The enzyme inhibitory activity of the compounds was calculated using the following formula:

$$\text{inhibition} = [(A_{\text{c}} - A_{\text{s}})/A_{\text{c}}] \times 100$$

where  $A_{\text{c}}$  is the absorbance of the control sample and  $A_{\text{s}}$  is the absorbance the test sample in the presence of an inhibitor.

The IC<sub>50</sub> values were determined using nonlinear regression from “absorbance vs concentration” curves generated from the data obtained for each inhibition assay, using Graph Pad Prism Version 7 (V<sub>7</sub>).

**Cell Culture and Maintenance.** Human hepatoma cell lines (HepG2) purchased from American Type Culture Collection (ATCC) were cultured and maintained following standard protocols and procedures. The cells were maintained and cultured in complete medium [Dulbecco's modified minimal essential medium (DMEM) supplemented with 10% (v/v) of fetal bovine serum (FBS) and 1% antibiotics (v/v)]. Standard cell culture maintenance was followed (incubation at 37 °C

Table 6. Primer Sequences of LDL Uptake Related Genes

gene	forward (5'-3')	reverse (5'-3')
GAPDH	TCCTGTTTCGACAGTCAGCCG	CCCCATGGTGTCTGAGCGAT
PCSK 9	CGGTACCGGGCGGATGAATA	CCTCGATTTCGGTGGTCA
LDLR	CAGGACGGCTACAGCTACCC	CAGGCAGATGTTACGCCAC
SREBP-2	CCCCCGGTCTCCCTGAG	ACAAGTCAGGGAAGTCTCCAC
HMGCR	GGTTCGGTGGCCTCTAGTGA	AGGGATGGGAGGCCACAAG

with 5% CO<sub>2</sub> until 70–80% confluent) with splitting at 3–4 days intervals.

**Cellular Toxicity.** HepG2 cells (at 70–80% confluence) were seeded at a concentration of  $5.0 \times 10^4$  per 100  $\mu$ L in a 96-well plate and cultured for 24 h at 37 °C and 5% CO<sub>2</sub>. On the next day, the cells were exposed to the test compound (1–100  $\mu$ M), while the control cells were either exposed to 0.01% methanol (vehicle control) and PBS and further incubated for 72 h at 37 °C and 5% CO<sub>2</sub>. The cells were then fixed with 20% formalin (final concentration 2%) (v/v) and incubated at 37 °C for 30 min. The medium was discarded, and the plate was blotted dry. This was followed by addition of 100  $\mu$ L of crystal violet (0.1% in 200 mM formic acid) to the plate and allowed to stand for 30 min at room temperature. The dye was then removed, and the plate was washed well with tap water and then dried. The attached cells were stained with crystal violet. The dye was then extracted with 100  $\mu$ L of 10% acetic acid (v/v), and the absorbance was read at 630 nm. The results were expressed as the percentage cell number relative to the control (cells treated with PBS).

**Cellular LDL Uptake Assay in HepG2 Cells.** Cellular LDL uptake was determined as described by ref 28. Briefly, HepG2 cells ( $5.0 \times 10^4$  per 100  $\mu$ L) were seeded and cultured as described above for 48 h. Then, the cells were exposed for 48 h to the test compounds (triterpenoids) at 25 and 100  $\mu$ M, with cells exposed to 0.01% methanol (vehicle control) and sterile PBS served as the controls. The culture medium was then substituted with LDL-DyLight 550 working solution followed by 2 h incubation at 37 °C. The LDL-DyLight 550 was then aspirated and replaced with 100  $\mu$ L of PBS. The degree of cellular LDL uptake was determined by measuring the intracellular LDL-DyLight fluorescence at 540 nm (excitation) and 570 nm (emission).

**Real-Time q-RT-PCR Analysis.** The effect of the triterpenoids on the expression of some genes such as SREBP-2, LDLR, PCSK-9, and HMG CoA reductase, which are associated with cellular LDL uptake, was studied using real-time q-RT-PCR.<sup>7</sup> HepG2 cells were cultured and treated as described for the cellular LDL uptake above. Total RNA from the cells was extracted using an RNA extraction kit (Promega) and converted to cDNA using the iScript cDNA synthesis kit (Promega) as described in the manufacturer's protocols. The synthesized cDNA was used for real-time q-RT-PCR analysis with Go Taq qPCR Master Mix. The gene-specific primers (Inqaba Biotech) were used for quantitative PCR using Bio-Rad CFX Maestro software. Each real-time PCR (20  $\mu$ L total volume) contained 2  $\mu$ L of cDNA template, 10  $\mu$ L of Go Taq qPCR Master Mix, 2  $\mu$ L of each of the forward and reverse primers (Table 1), 0.2  $\mu$ L of CXR reference dye, and 3.98  $\mu$ L of nuclease-free water. The standard cycling conditions (40 cycles) involved denaturation at 95 °C for 15 s and annealing at 60 °C and extension for 1 min. All mRNA expression levels were normalized to glyceraldehyde 3-phosphate dehydrogenase (GAPDH). The primers were designed from the BLAST

NCBI online server (<https://www.ncbi.nlm.nih.gov/tools/primer-blast/>) (Table 6).

**Construction of the Protein–Protein Interaction Network.** The interrelationship between the overlapping genes in physiological and pathophysiological states can be revealed by establishing a protein–protein interaction (PPI) network. Studying PPI is a vital strategy to identify core regulatory genes within a cell. The STRING database (<https://string-db.org/>), which covers abundant information regarding known and predicted protein–protein interactions of different species,<sup>29</sup> was accessed to obtain the PPI information between the four genes: *LDLR*, *SREBP2*, *PCSK9*, and *HMGCR*. Parameters including the average node degree (the number of interactions that a protein has on average in the network) and clustering coefficients (the measure of how connected the nodes in the network are) are very important in completing the PPI network analysis. To build the interaction network, a high confidence score > 0.7 was reserved to ensure accuracy and reliability, and the species was limited to *Homo sapiens*. Subsequently, the PPI network obtained was visualized and analyzed using Cytoscape software version 3.9.1.

## STATISTICAL ANALYSIS

Unless otherwise stated, all the experiments were replicated at least three times. The results were expressed as mean  $\pm$  SEM of three biological repeats. Multiple comparisons of the data were performed by one-way analysis of variance (ANOVA) followed by Dunnett *post hoc* tests using Graph Pad Prism Version 7 (V<sub>7</sub>). Statistical difference was considered significant where  $p < 0.05$ .

## ASSOCIATED CONTENT

### Supporting Information

The Supporting Information is available free of charge at <https://pubs.acs.org/doi/10.1021/acsomega.3c01995>.

(PDF)

## AUTHOR INFORMATION

### Corresponding Authors

Musawenkosi Ndlovu – Department of Biochemistry, Genetics and Microbiology, University of Pretoria, Hatfield 0028, South Africa; [orcid.org/0000-0002-5901-6766](https://orcid.org/0000-0002-5901-6766); Email: [muser165@gmail.com](mailto:muser165@gmail.com)

Rebamang A. Mosa – Department of Biochemistry, Genetics and Microbiology, University of Pretoria, Hatfield 0028, South Africa; Email: [rebamang.mosa@up.ac.za](mailto:rebamang.mosa@up.ac.za)

### Authors

June C. Serem – Department of Anatomy, University of Pretoria, Pretoria 0007, South Africa

Mamoalosi A. Selepe – Department of Chemistry, University of Pretoria, Hatfield 0028, South Africa; [orcid.org/0000-0002-5081-178X](https://orcid.org/0000-0002-5081-178X)

Andrew R. Opoku – Department of Biochemistry and Microbiology, University of Zululand, KwaDlangezwa 3886, South Africa

Megan J. Bester – Department of Anatomy, University of Pretoria, Pretoria 0007, South Africa

Zeno Apostolides – Department of Biochemistry, Genetics and Microbiology, University of Pretoria, Hatfield 0028, South Africa

Complete contact information is available at:

<https://pubs.acs.org/10.1021/acsomega.3c01995>

## Notes

The authors declare no competing financial interest.

## ACKNOWLEDGMENTS

The authors are grateful to the University of Pretoria. The work was financially supported by the South African National Research Foundation (grant numbers (UID): 121928 and 123589).

## REFERENCES

- (1) The World Health Organization *Cardiovascular diseases (CVDs)*, 2021. [https://www.who.int/news-room/fact-sheets/detail/cardiovascular-diseases-\(cvds\)](https://www.who.int/news-room/fact-sheets/detail/cardiovascular-diseases-(cvds)) (accessed March 17, 2023).
- (2) Mortensen, M. B.; Nordestgaard, B. G. Elevated LDL cholesterol and increased risk of myocardial infarction and atherosclerotic cardiovascular disease in individuals aged 70–100 years: a contemporary primary prevention cohort. *The Lancet* **2020**, *396*, 1644–1652.
- (3) Jiang, J.; Wu, C.; Zhang, C.; Zhang, Q.; Yu, L.; Zhao, J.; Zhang, H.; Narbad, A.; Chen, W.; Zhai, Q. Strain-specific effects of *Bifidobacterium longum* on hypercholesterolemic rats and potential mechanisms. *Int. J. Mol. Sci.* **2021**, *22*, 1305–1322.
- (4) Su, J.; Wang, H.; Ma, C.; Liu, C.; Gao, C.; Nie, R.; Tanver Rahman, M. R. Hypocholesterolaemic mechanism of bitter melon aqueous extracts via inhibition of pancreatic cholesterol esterase and reduction of cholesterol micellar solubility. *Int. J. Food Sci. Nutr.* **2016**, *67*, 20–28.
- (5) Iqbal, J.; Al Qarni, A.; Hawwari, A. Regulation of intestinal cholesterol absorption: a disease perspective. *Adv. Biol. Chem.* **2017**, *07*, 60–75.
- (6) Joyce, S. A.; Kamil, A.; Fleige, L.; Gahan, C. G. The cholesterol-lowering effect of oats and oat beta glucan: modes of action and potential role of bile acids and the microbiome. *Front. Nutr.* **2019**, *6*, 171–186.
- (7) Choi, Y. J.; Lee, S. J.; Kim, H. I.; Lee, H. J.; Kang, S. J.; Kim, T. Y.; Cheon, C.; Ko, S. G. Platycodin D enhances LDLR expression and LDL uptake via down-regulation of IDOL mRNA in hepatic cells. *Sci. Rep.* **2020**, *10*, 1–13.
- (8) Schonewille, M.; de Boer, J. F.; Mele, L.; Wolters, H.; Bloks, V. W.; Wolters, J. C.; Kuivenhoven, J. A.; Tietge, U. J.; Brufau, G.; Groen, A. K. Statins increase hepatic cholesterol synthesis and stimulate fecal cholesterol elimination in mice. *J. Lipid Res.* **2016**, *57*, 1455–1464.
- (9) Raghov, R. Statins redux: A re-assessment of how statins lower plasma cholesterol. *World J. Diabetes* **2017**, *8*, 230–234.
- (10) Horodinschi, R. N.; Stanescu, A. M. A.; Bratu, O. G.; Pantea Stoian, A.; Radavoi, D. G.; Diaconu, C. C. Treatment with statins in elderly patients. *Medicina* **2019**, *55*, 721–732.
- (11) Graf, B. L.; Raskin, I.; Cefalu, W. T.; Ribnicky, D. M. Plant-derived therapeutics for the treatment of metabolic syndrome. *Curr. Opin. Invest. Drugs* **2010**, *11*, 1107–1116.
- (12) Mamadalieva, N. Z.; Youssef, F. S.; Hussain, H.; Zengin, G.; Mollica, A.; Al Musayeb, N. M.; Ashour, M. L.; Westermann, B.; Wessjohann, L. A. Validation of the antioxidant and enzyme inhibitory potential of selected triterpenes using in vitro and in silico studies, and the evaluation of their ADMET properties. *Molecules* **2021**, *26*, 6331–6350.
- (13) Machaba, K. E.; Cobongela, S. Z.; Mosa, R. A.; Oladipupo, L. A.; Djarova, T. G.; Opoku, A. R. *In vivo* anti-hyperlipidemic activity of the triterpene from the stem bark of *Protorhus longifolia* (Benrh) Engl. *Lipids Health Dis.* **2014**, *13*, 1–7.
- (14) Mosa, R. A.; Naidoo, J. J.; Nkomo, F. S.; Mazibuko, S. E.; Muller, C. J.; Opoku, A. R. In vitro antihyperlipidemic potential of triterpenes from stem bark of *Protorhus longifolia*. *Planta Med.* **2014**, *80*, 1685–1691.
- (15) Mosa, R. A.; Oyedeji, A. O.; Shode, F. O.; Singh, M.; Opoku, A. R. Triterpenes from the stem bark of *Protorhus longifolia* exhibit anti-platelet aggregation activity. *Afr J Pharm Pharmacol* **2011**, *5*, 2698–2714.
- (16) Verhoff, M.; Seitz, S.; Paul, M.; Noha, S. M.; Jauch, J.; Schuster, D.; Werz, O. Tetra- and pentacyclic triterpene acids from the ancient anti-inflammatory remedy frankincense as inhibitors of microsomal prostaglandin E<sub>2</sub> synthase-1. *J. Nat. Prod.* **2014**, *77*, 1445–1451.
- (17) Santos, F. A.; Frota, J. T.; Arruda, B. R.; de Melo, T. S.; de Castro Brito, G. A.; Chaves, M. H.; Rao, V. S. Antihyperglycemic and hypolipidemic effects of  $\alpha$ ,  $\beta$ -amyryn, a triterpenoid mixture from *Protium heptaphyllum* in mice. *Lipids Health Dis.* **2012**, *11*, 1–8.
- (18) Jesch, E. D.; Carr, T. P. Food ingredients that inhibit cholesterol absorption. *Prev. Nutr. Food Sci.* **2017**, *22*, 67–80.
- (19) Ilias, A. N.; Ismail, I. S.; Hamzah, H.; Mohidin, T. B. M.; Idris, M. F.; Ajat, M. Rebaudioside A enhances LDL cholesterol uptake in HepG2 cells via suppression of HMGCR expression. *Rep. Biochem. Mol. Biol.* **2021**, *10*, 477–487.
- (20) Hwang, J. T.; Choi, E.; Choi, H. K.; Park, J. H.; Chung, M. Y. The cholesterol-lowering effect of *Capsella Bursa-Pastoris* is mediated via SREBP2 and HNF-1 $\alpha$ -regulated PCSK9 inhibition in obese mice and HepG2 cells. *Foods* **2021**, *10*, 408–422.
- (21) Sultan, M. A.; Galil, M. S.; Al-Qubati, M.; Omar, M. M.; Barakat, A. Synthesis, molecular docking, druglikeness analysis, and ADMET prediction of the chlorinated ethanoanthracene derivatives as possible antidepressant agents. *Appl. Sci.* **2020**, *10*, 7727–7746.
- (22) Takomthong, P.; Waiwut, P.; Yenjai, C.; Sombatsri, A.; Reubroycharoen, P.; Lei, L.; Lai, R.; Chaiwiwatrakul, S.; Boonyarat, C. Multi-target actions of acridones from *Atalantia monophylla* towards Alzheimer's pathogenesis and their pharmacokinetic properties. *Pharmaceuticals* **2021**, *14*, 888–908.
- (23) Saeed, M.; Tasleem, M.; Shoib, A.; Kausar, M. A.; Sulieman, A. M. E.; Alabdallah, N. M.; El Asmar, Z.; Abdelgadir, A.; Al-Shammari, A.; Alam, M. J.; Badroui, R. Identification of putative plant-based ALR-2 inhibitors to treat diabetic peripheral neuropathy. *Curr. Issues Mol. Biol.* **2022**, *44*, 2825–2841.
- (24) Pires, D. E.; Blundell, T. L.; Ascher, D. B. pkCSM: predicting small-molecule pharmacokinetic and toxicity properties using graph-based signatures. *J. Med. Chem.* **2015**, *58*, 4066–4072.
- (25) Abeysekera, W. P. K. M.; Arachchige, S. P. G.; Ratnasooriya, W. D. Bark extracts of Ceylon cinnamon possess antilipidemic activities and bind bile acids in vitro. *Evidence-Based Complementary and Alternative Medicine*, 2017 **2017**, 1–10.
- (26) Salvamani, S.; Gunasekaran, B.; Shukor, M. Y.; Shaharuddin, N. A.; Sabullah, M. K.; Ahmad, S. A. Anti-HMG-CoA reductase, antioxidant, and anti-inflammatory activities of *Amaranthus viridis* leaf extract as a potential treatment for hypercholesterolemia. *Evidence-Based Complementary and Alternative Medicine*, 2016 **2016**, 1–10.
- (27) Zhang, H.; Yokoyama, W. H.; Zhang, H. Concentration-dependent displacement of cholesterol in micelles by hydrophobic rice bran protein hydrolysates. *J. Sci. Food Agric.* **2012**, *92*, 1395–1401.
- (28) Lammi, C.; Zannoni, C.; Arnoldi, A.; Vistolli, G. Two peptides from soy  $\beta$ -conglycinin induce a hypocholesterolemic effect in HepG2 Cells by a statin-like mechanism: Comparative in vitro and in silico modeling studies. *J. Agric. Food Chem.* **2015**, *63*, 7945–7951.
- (29) Szklarczyk, D.; Morris, J. H.; Cook, H.; Kuhn, M.; Wyder, S.; Simonovic, M.; Santos, A.; Doncheva, N. T.; Roth, A.; Bork, P.;

Jensen, L. J. The STRING database in 2017: quality-controlled protein–protein association networks, made broadly accessible. *Nucleic Acids Res.* **2016**, gkw 937.